Communication

Cuprous Halide Coordination Polymer for Efficient NIR-I Photothermal Effect and Photo-thermo-electric Conversion

Ning-Ning Zhang *, Xiang-Tong Liu , Ke Xu , Ya-Tong Liu , Lin-Xu Liu , Yong Yan *

Posted Date: 22 November 2024

doi: 10.20944/preprints202411.1687.v1

Keywords: Cuprous halide coordination polymers; black photothermal agent; near infrared photothermal effects; photo-thermo-electric conversion

 doi:10.20944/preprints202411.1687.v1

Communication

Cuprous Halide Coordination Polymer for Efficient NIR-I Photothermal Effect and Photo-Thermo-Electric Conversion

Ning-Ning Zhang *, Xiang-Tong Liu, Ke Xu, Ya-Tong Liu, Lin-Xu Liu and Yong Yan *

School of Chemistry and Chemical Engineering, Liaocheng University, Liaocheng, Shandong 252000, China
* Correspondence: zhangningning@lcu.edu.cn; yanyong@lcu.edu.cn.

Abstract: Photo-thermo-electric conversion devices represent a promising technology for converting solar energy into electrical energy. Photothermal materials, as a critical component, play a significant role in efficient conversion from solar energy to thermal energy and subsequently to electrical energy, thereby directly influencing the overall system's solar energy utilization efficiency. However, the application of single-component photothermal materials in photo-thermo-electric conversion systems remains limited. The exploration of novel photothermal materials with broad-spectrum absorption, high photothermal conversion efficiency (PCE), and robust output power density is highly desired. In this study, we investigated a black cuprous halide compound, $[Cu_2Cl_2PA]_n$ (**1**, **PA** = phenazine), which exhibits broad-spectrum absorption extending into the near-infrared (NIR) region. Compound **1** demonstrated a high NIR-I PCE of 50% under irradiation of an 808 nm laser, attributed to metal-to-ligand charge transfer (MLCT) from Cu(I) to **PA** ligands and strong intermolecular π–π interactions among **PA** ligands. Furthermore, the photo-thermo-electric conversion device constructed using compound **1** achieved a notable output voltage of 261 mV and an output power density of 0.92 W/m² under the 1 Sun (1000 W/m²) xenon lamp.

Keywords: Cuprous halide coordination polymers; black photothermal agent; near infrared photothermal effects; photo-thermo-electric conversion

1. Introduction

Solar energy, as a ubiquitous and abundant green energy resource, offers significant potential to reduce pollution, mitigate global warming, and alleviate the pressures arising from fossil fuel scarcity [1,2]. Among the various solar energy utilization technologies, photo-thermo-electric conversion has emerged as a promising approach for directly converting solar energy into electrical energy, garnering substantial attention [3]. This technology relies on the synergistic interplay of two fundamental energy conversion processes: photothermal conversion and thermoelectric conversion based on the Seebeck effect [4]. Upon solar irradiation, photothermal materials convert light energy into thermal energy, creating a temperature difference (ΔT) across the thermoelectric device. This temperature gradient drives the generation of a potential difference within the thermoelectric device, enabling the production of electrical energy. Photo-thermo-electric conversion devices offer several advantages, including a wide response wavelength range, self-sustainability, miniaturization, and portability [5]. These attributes make them particularly suitable for applications such as outdoor power generation, remote area power supplies, wearable electronics, and space exploration [6].

Photothermal materials, as a critical component of photo-thermo-electric conversion devices, play a pivotal role in enabling the efficient transformation of solar energy into thermal energy and subsequently into electrical energy, directly impacting the overall system's solar energy utilization efficiency. Among the reported photo-thermo-electric conversion devices, the employed photothermal materials predominantly consist of composite nanomaterials based on metals [7–9], carbon [10–12], and polymers [13]. While these materials hold promise, their applications are hindered by limitations such as low output voltage and power density (Table S1). Recently, single-

 doi:10.20944/preprints202411.1687.v1

component broad-spectrum absorbing photothermal materials, including donor-acceptor (D-A) organic co-crystals [**Error! Bookmark not defined.**], D-A organic molecules [14], and inorganic-organic hybrids [15,16], have started to gain attention in the context of photo-thermo-electric conversion. Notably, the output power densities of these single-component materials are generally higher than those of composite materials (Table S1). However, the application of single-component photothermal materials in this field remains limited to a few examples. Therefore, the development of novel single-component photothermal materials with broad-spectrum absorption, high photothermal conversion efficiency (PCE), and robust output power density continues to be a significant challenge.

Photothermal conversion is essentially a non-radiative transition process from an excited state to a ground state [17]. Hence, numerous strategies that affect this photophysical process can enhance the PCE of the compound, such as intermolecular π–π interactions [18], molecular motion [19], charge transfer [20], fluorescence resonance energy transfer [21], photoinduced electron transfer [22], and the heavy atom effect [23]. Among these, the formation of charge transfer states has been particularly attractive, as it not only broadens optical absorption but also facilitates the non-radiative decay of excited states. To date, many efficient photothermal materials with broad-spectrum absorption have been developed by realizing low-energy charge transfer states in organic systems [24,25]. In fact, in addition to organic systems, low-energy charge transfer states are also prevalent in organic-inorganic hybrids [26], particularly in cuprous complexes [27]. According to previous studies [28], Cu(I) complexes usually form metal-to-ligand charge transfer (MLCT) states when coordinated with electron-deficient ligands under light irradiation, and their optical features can be tailored by refining the molecular structure and energy levels of the ligands. Inspired by these characteristics, we selected a cuprous halide coordination polymer (**1**, $[Cu_2Cl_2PA]_n$, **PA** = phenazine) from the Cambridge Crystallographic Data Centre (CCDC) database as the research object in this work. Compound **1** is black in appearance and exhibits a broad optical absorption band extending into the near-infrared (NIR) region. Experimental results revealed that compound **1** achieves a high NIR-I photothermal conversion efficiency (50 %) under 808 nm laser irradiation, attributed to MLCT from Cu(I) to **PA** ligands and strong intermolecular π-π interactions among **PA** ligands. Furthermore, a photo-thermal-electric conversion device based on compound 1 demonstrated excellent performance, achieving an output voltage of 261 mV and a power density of 0.92 W/m² under 1 Sun (1000 W/m²) illumination.

2. Results and Discussion

Compound **1** was synthesized using a novel solvothermal one-step method, which is simple, efficient, and yields a high product quantity (detailed procedures are provided in the Supporting Information). This approach offers significant advantages over the previously reported method, which required synthesis under an argon atmosphere, making it more complex and time-consuming [29]. The phase purity of compound **1** was confirmed by powder X-ray diffraction (PXRD) (Figure S1) spectroscopy. Additionally, thermogravimetric (TG) analysis revealed that the crystal sample of compound **1** exhibits good thermal stability, with no obvious weight loss observed before 210 °C (Figure S2). Structural analysis indicates that compound **1** adopts a two-dimensional layer structure with a polymeric stair-like framework. The copper atoms are coordinated in a distorted tetrahedral geometry, bonded to one nitrogen atom from the **PA** ligand and three chloride ions. Figure 1a depicts the *b*-axis view of the two-dimensional layer, with an interplanar spacing of 3.36 Å among **PA** ligands.

 doi:10.20944/preprints202411.1687.v1

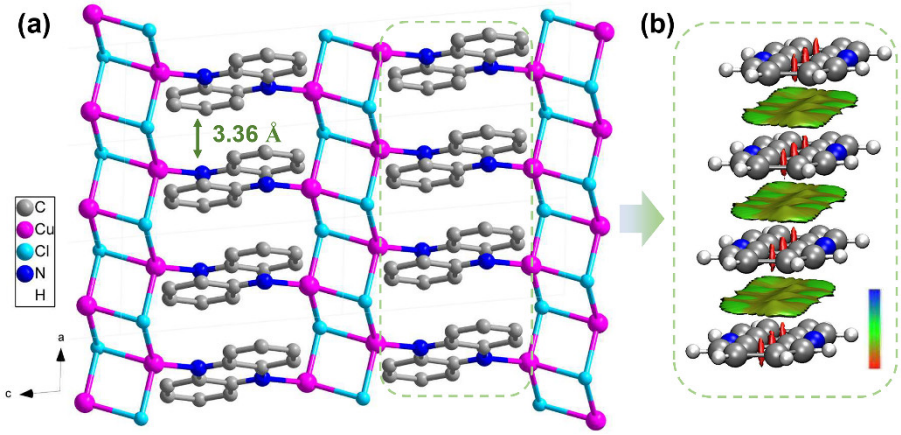

Figure 1. (a) The 2D layer structure of compound **1** as viewed along the *b* axis. (b) A selected π–π stacking fragment within compound **1**, along with its calculated gradient isosurfaces (s = 0.5 a.u.). The surfaces are colored using a blue-green-red (BGR) scale based on the values of sign(λ_2)ρ, which range from –0.04 to 0.02 a.u.. In this scale, blue indicates strong attractive interactions, green represents moderate attractive interactions, and red signifies strong non-bonded overlaps.

Interestingly, the crystalline powder sample of compound **1** appears black under ambient conditions (Figure 2a). Solid-state UV-Vis-NIR spectra reveal that compound **1** exhibits a broad optical absorption band spanning from the ultraviolet to the near-infrared region, with an absorption edge extending to 1200 nm, in contrast to the ligand **PA**. (Figure 2a). To investigate the origin of this broad absorption spectrum, the absorption peaks were analyzed and assigned. The absorption peaks at 363 nm and 480 nm were attributed to the intrinsic absorption of the **PA** ligand. Density of states (DOS) and partial DOS (PDOS) calculations indicated that the Γ_a and Γ_c states primarily arise from the mixed antibonding p_π orbitals of **PA** ligands, while the Γ_b states originate from the *d* orbitals of Cu(I) (Figure 2b, S3). As a result, the absorption peak at 538 nm (2.3 eV) was attributed to the transfer from Γ_a state to Γ_c state, corresponding to ligand-to-ligand charge transfer (LLCT) among **PA** ligands. The absorption peak at 710 nm (1.746 eV) was attributed to the transfer from Γ_b state to Γ_c state, corresponding to metal-to-ligand charge transfer (MLCT) from Cu(I) to **PA** ligands (Figure 2b, S3). And strong intermolecular π–π interactions among coordinated **PA** ligands (Figure 1b) may further extend and broaden the absorption edge [30]. Therefore, the broad-spectrum absorption of compound **1** results from the combined contributions of MLCT and intermolecular π–π interactions.

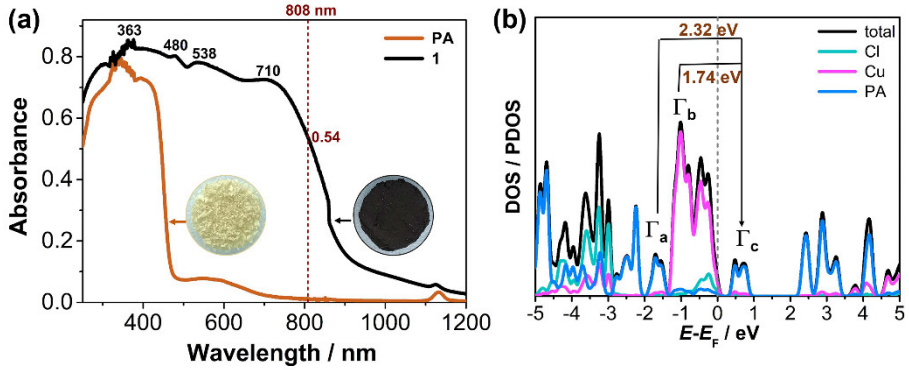

Figure 2. (a) Solid-state absorption spectra of **PA** and compound **1**. (b) TDOS and PDOS of **1**, with the Fermi level (E_F) set to zero as a reference.

Encouraged by the strong absorption in the near-infrared (NIR) region and the high thermal stability of **1**, a detailed investigation into its NIR-I photothermal conversion properties was conducted. Upon irradiation with an 808 nm laser (0.75 W/cm²), the temperature of crystalline pellets rapidly increased from 27.3 °C to approximately 91.5 °C (Figure S4). In contrast, no significant temperature rise was observed on a blank quartz glass plate under the same conditions (Figure S4).

 doi:10.20944/preprints202411.1687.v1

When the power of the 808 nm laser was varied to 0.125, 0.25, 0.375, 0.50, 0.625, and 0.75 W·cm^{-2}, the corresponding temperatures of the crystalline pellets were 43.4, 52.4, 59.3, 70.4, 81.0, and 91.5 °C, respectively, demonstrating a linear response of the photothermal effects of compound **1** (Figure 3a, 3b). The maximum temperature changes (ΔT_{max}) for these conditions were 14.7, 24.2, 31.5, 42.4, 53.4, and 64.2 K, respectively (Figure 3a, 3b). To assess the stability and durability of the photothermal conversion, cycling experiments were performed under an 808 nm laser with a power density of 0.75 W/cm^2. The results demonstrated that the photothermal effects of compound **1** remained stable for at least six cycles (Figure 3c). Furthermore, based on the cooling curves and corresponding time-lnθ linear analysis (Figure S5), the photothermal conversion efficiency (PCE, η) of compound **1** was estimated to be 50 %. Moreover, previous studies have shown that charge transfer and intermolecular π–π interactions can lead to denser electronic energy levels in molecules, thereby facilitating nonradiative decay of excited states through increased vibrational cooling and internal conversion. As a result, the MLCT and intermolecular π–π interactions in compound **1** are assumed to contribute significantly to its efficient photothermal conversion when irradiated with an 808 nm laser.

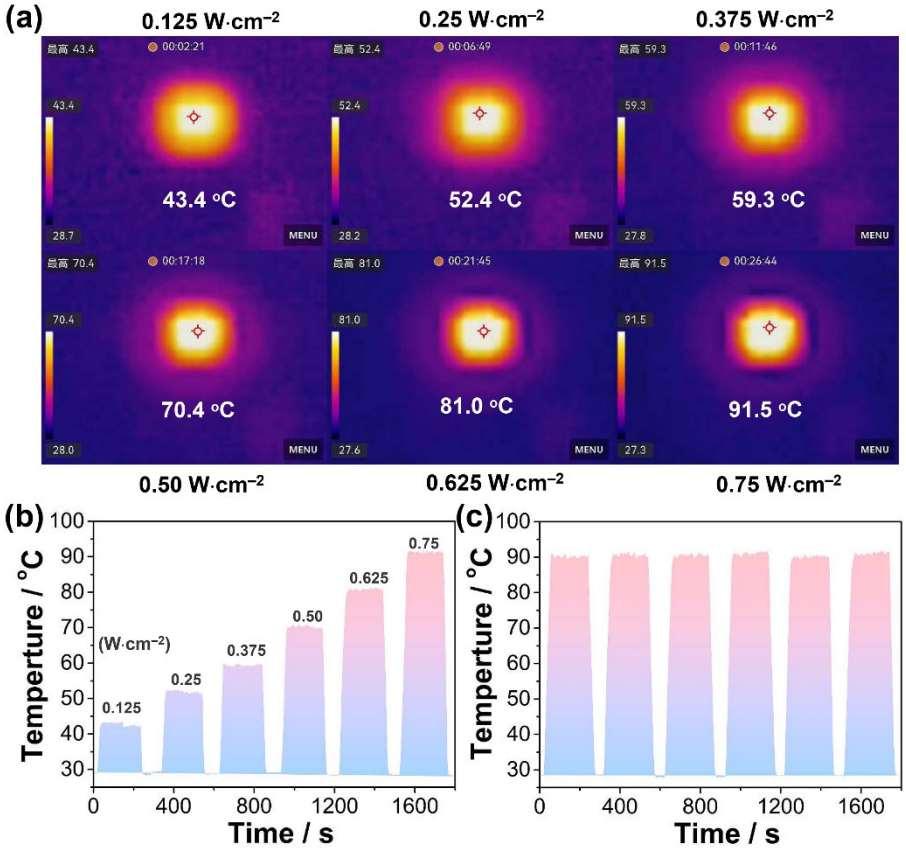

Figure 3. (a) Infrared images of the crystalline pellet of **1** under varying irradiation power density. (b) Temperature variations of **1** under 808 nm laser irradiation at different power densities. (c) Cycling temperature profile of **1** under 808 nm laser irradiation with a constant power density of 0.75 W/cm^2.

Given its broad absorption band and efficient NIR-I photothermal effect, the application of compound **1** in photo-thermo-electric conversion was investigated. About 50 mg sample of crystalline powder of compound **1** was evenly applied to the surface of a commercial thermoelectric generator (TEC1-12701) using thermal conductive glue (Figure 4a). Under 1 Sun irradiation provided by a solar simulator system (CEL-PF300-T9), the device **1**@TEC1-12701 exhibited an open-circuit voltage of 261 mV (Figure 4c) and an output current of 16.0 mA (Figure 4f). To further assess the performance, compound **1** was tested with two other commercially available thermoelectric generators, TEC1-12703 and TEC1-12706. The results showed that after coating the devices with the same weight of crystalline powder of **1**, under 1 Sun irradiation, the open-circuit voltage and current of **1**@TEC1-12703 were 142 mV and 22.5 mA (Figure 4d, 4g), respectively. For **1**@TEC1-12706, the

 doi:10.20944/preprints202411.1687.v1

open-circuit voltage and current were 86 mV and 25.4 mA (Figure 4e, 4h), respectively. Temperature measurements revealed negligible temperature changes of less than 1 K for the blank thermoelectric generators (Figure S6a). However, after applying the crystalline powder of **1**, temperature differences were observed to increase, indicating that the **1**-coated layers act as efficient photothermal materials. Although the applied weight of the sample was consistent, **1**@TEC1-12701 exhibited the largest temperature difference of 9 K (Figure S6a), highlighting the importance of the coating process in achieving high photo-thermo-electric conversion efficiency. Moreover, **1**@TEC1-12703 and **1**@TEC1-12706 had similar case (Figure S6b, S6c). As reported, open-circuit voltage and current are proportional to the intensity of radiation. To further improve the output performance, the radiation intensity was increased to 2 Suns (2000 W/m²). Under these conditions, both the open-circuit voltage and current were enhanced (Figure 4c–4h). Notably, **1**@TEC1-12701 showed a maximum open-circuit voltage of 392 mV (Figure 4c) and a current of 20.0 mA (Figure 4f). These results suggest that higher solar radiation power density leads to better power generation performance. The performance of **1** in this system is comparable to that of reported inorganic-organic hybrid materials, indicating that metal halide of compound **1** holds significant potential for application in the field of photo-thermo-electric conversion.

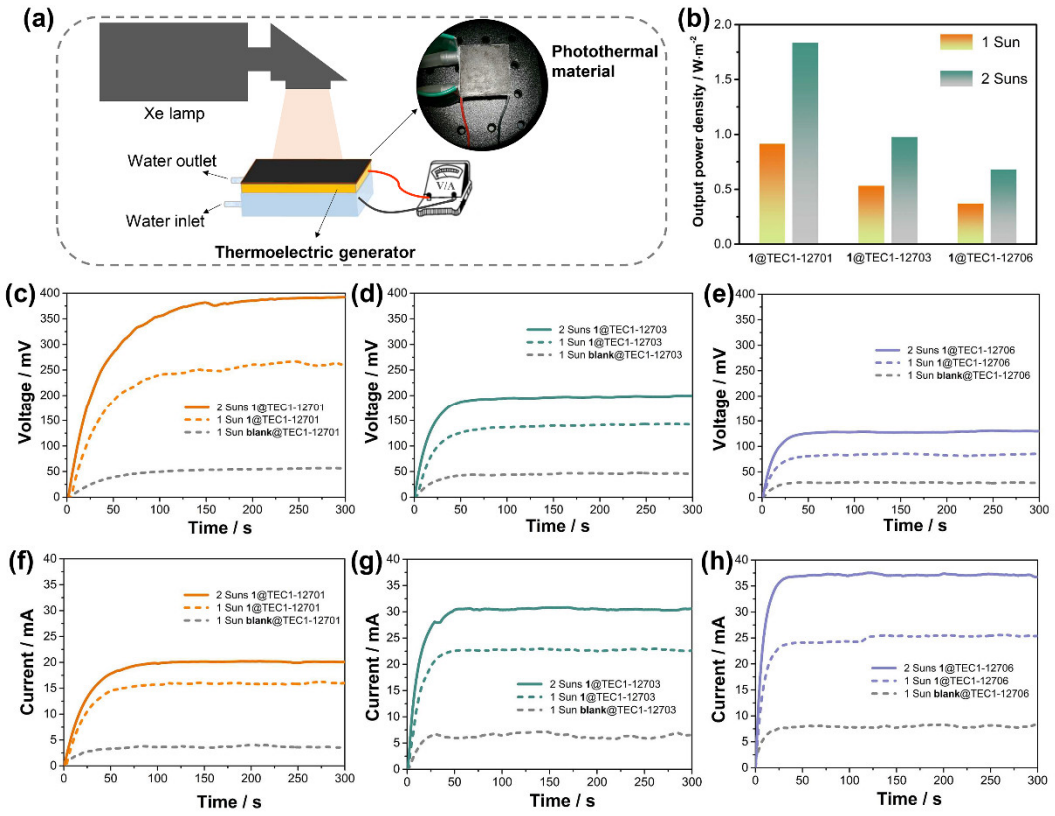

Figure 4. (a) Schematic diagram of photothermal-electric conversion device. (b) The output power density of different photo-thermo-electric conversion systems when loading external resistances under the irradiation of 1 Sun and 2 Suns. Open circuit voltages (c–e) and currents (f–h) of different commercial thermoelectric generators after loading compound **1** under the irradiation of 1 Sun and 2 Suns, respectively.

To evaluate the maximum output power of different thermoelectric generators coated with compound **1** under 1 Sun and 2 Suns irradiation, various external resistances were connected. The results showed that **1**@TEC1-12701 produced the highest power output when paired with an external resistance of 12.2 Ω (Figure S7), while **1**@TEC1-12703 and **1**@TEC1-12706 exhibited peak output power at resistances of 9.3 Ω and 3.2 Ω, respectively (Figure S8, S9). As shown in Figure 4b, **1**@TEC1-12701 demonstrated the highest output power density under both 1 Sun and 2 Suns irradiation, reaching 0.92 W/m² and 1.84 W/m², respectively. In comparison, under 1 Sun, **1**@TEC1-12703 and

 doi:10.20944/preprints202411.1687.v1

1@TEC1-12706 achieved maximum output power densities of 0.53 W/m² and 0.37 W/m² (Figure 4b), respectively. Under 2 Suns, these values increased to 0.98 W/m² and 0.68 W/m² (Figure 4b), respectively. Although the photo-thermo-electric conversion efficiency of **1**@TEC1-12701 is not the highest reported (Table S1), it surpasses that of the majority of photothermal materials reported to date.

3. Conclusions

In conclusion, this study presents the first demonstration of photo-thermo-electric conversion using a photothermal cuprous halide coordination polymer. The synergy between metal-to-ligand charge transfer (MLCT) from Cu(I) to **PA** ligands and strong intermolecular π–π interactions among the coordinated **PA** ligands enables compound **1** to exhibit a broad absorption band and a high NIR-I photothermal conversion efficiency (PCE) of 50% under an 808 nm laser irradiation. Furthermore, the photo-thermo-electric conversion device constructed with compound **1** (**1**@TEC1-12701) achieved a high output voltage of 261 mV and an notable output power density of 0.92 W/m² under 1 Sun (1000 W/m²) xenon lamp irradiation. Considering the excellent NIR-I photothermal conversion performance of compound **1**, this significantly enhances the potential of cuprous halide complexes in photo-thermo-electric conversion applications.

Supplementary Materials: The following supporting information can be downloaded at the website of this paper posted on Preprints.org. The general methods, materials and synthesis, computational details, and the additional table and graphics are provided in supporting information. Table S1: Reported photothermal materials and their performance in photo-thermo-electric conversion when integrating with thermoelectric generators under the irradiation of 1 Sun. Figure S1: PXRD patterns of compound **1** and simulated data using single-crystal data. Figure S2: TG curve of compound **1**. Figure S3: Partial DOS of Cu^{I} (a) and PA (b) in compound **1**. Figure S4: Temperature curves of **1** and blank quartz glass plate under the irradiation of 0.75 W/cm² 808 nm laser. Figure S5: Temperature decaying curve of compound **1** after removing the laser source of 808 nm (0.75 W/cm²) (a) and the corresponding time-lnθ linear curve (b). Figure S6: Temperature difference (ΔT) of different photo-thermo-electric conversion devices under the irradiation of 1 Sun. Figure S7: Output power of **1**@TEC1-12701 under irradiation of 1 Sun (a) and 2 Sun (b) when loading different external resistances. Figure S8: Output power of **1**@TEC1-12703 under irradiation of 1 Sun (a) and 2 Suns (b) when loading different external resistances. Figure S9: Output power of **1**@TEC1-12706 under irradiation of 1 Sun (a) and 2 Suns (b) when loading different external resistances.

Author Contributions: Investigation, N.-N. Zhang, X.-T. Liu and Y.-T. Liu; Data curation, L.-X. Liu and K. Xu; Writing—original draft, N.-N. Zhang; Writing—review & editing, Y. Yan; Supervision, N.-N. Zhang; Project administration, N.-N. Zhang; Funding acquisition, N.-N. Zhang and Y. Yan. All authors have read and agreed to the published version of the manuscript.

Funding: This research was funded by the Natural Science Foundation of Shandong Province (ZR2022QB041 and ZR2023QB195).

Institutional Review Board Statement: Not applicable.

Informed Consent Statement: Not applicable.

Data Availability Statement: The original contributions presented in this study are included in the article/supplementary material. Further inquiries can be directed to the corresponding author(s).

Acknowledgments: The authors would like to thank all the reviewers who participated in the review. And we also thank Bianshui Riverside Supercomputing Center (BRSC) for calculation work.

Conflicts of Interest: The authors declare no conflicts of interest.

Reference

1. Fan, Z.; Ren, J.; Bai, H.; He, P.; Hao, L.; Liu, N.; Chen, B.; Niu, R.; Gong, J. Shape-Controlled Fabrication of MnO/C Hybrid Nanoparticle from Waste Polyester for Solar Evaporation and Thermoelectricity Generation. *Chem. Eng. J.* **2023**, *451*, 138534.
2. Gui, J.; Li, C.; Cao, Y.; Liu, Z.; Shen, Y.; Huang, W.; Tian, X. Hybrid Solar Evaporation System for Water and Electricity Co-Generation: Comprehensive Utilization of Solar and Water Energy. *Nano Energy* **2023**, 107, 108155.

3. Zhang, Q.; Huang, A.; Ai, X.; Liao, J.; Song, Q.; Reith, H.; Cao, X.; Fang, Y.; Schierning, G.; Nielsch, K.; Bai, S.; Chen, L. Transparent Power-Generating Windows Based on Solar-Thermal-Electric Conversion. *Adv. Energy Mater.* **2021**, *11*, 2101213.
4. He, J.; Tritt, T.M. Advances in thermoelectric materials research: Looking back and moving forward. *Science* **2017**, *357*, 1369.
5. Kraemer, D.; Hu, L.; Muto, A.; Chen, X.; Chen, G.; Chiesa, M. Photovoltaic-Thermoelectric Hybrid Systems: A General Optimization Methodology. *Appl. Phys. Lett.* **2008**, *92*, 243503.
6. Huang, Q.; Ye, X.; Chen, W.; Song, X.; Chen, Y.; Wen, X.; Zhang, M.; Wang, Y.; Chen, S.L.; Dang, L.; Li. M.D. Boosting Photo-thermo-electric Conversion via a Donor−Acceptor Organic Cocrystal Strategy. *ACS Energy Lett.* **2023**, *8*, 4179–4185.
7. Ren, J.; Ding, Y.; Gong, J.; Qu, J.; Niu, R. Simultaneous Solar-driven Steam and Electricity Generation by Cost-effective, Easy Scale-up MnO_2-based Flexible Membranes. *Energy Environ. Mater.* **2023**, *6*, e12376.
8. Fan, Z.; Ren, J.; Bai, H.; He, P.; Hao, L.; Liu, N.; Chen, B.; Niu, R.; Gong. J. Shape-controlled fabrication of MnO/C hybrid nanoparticle from waste polyester for solar evaporation and thermoelectricity generation. *Chem. Eng. J.* **2023**, *451*, 138534.
9. Li, N.; Yang, D. J.; Shao, Y.; Liu, Y.; Tang, J.; Yang, L.; Sun, T.; Zhou, W.; Liu, H.; Xue, G. Nanostructured Black Aluminum Prepared by Laser Direct Writing as a High-Performance Plasmonic Absorber for Photothermal/Electric Conversion. *ACS Appl. Mater. Interfaces* **2021**, *13*, 4305−4315.
10. Duan, Y.; Weng, M.; Zhang, W.; Qian, Y.; Luo, Z.; Chen, L. Multi-functional carbon nanotube paper for solar water evaporation combined with electricity generation and storage. *Engeg. Convers Manage.* **2021**, *241*, 114306.
11. Ghaffar, A.; Imran, Q.; Hassan, M.; Usman, M.; Khan, M. U. Simultaneous solar water desalination and energy generation by high efficient graphene oxide-melanin photothermal membrane. *J. Environ. Chem. Eng*. **2022**, *10*, 108424.
12. Wu, Y.; Li, Y.; Long, Y.; Xu, Y.; Yang, J.; Zhu, H.; Liu, T.; Shi, G. High-Efficiency Photo-Thermo-Electric System with Waste Heat Utilization and Energy Storage. *ACS Appl. Mater. Interfaces* **2022**, *14*, 40437–40446.
13. Lin, Z.; Wu, T.; Feng, Y.F.; Shi, J.; Zhou, B.; Zhu, C.; Wang, Y.; Liang, R.; Mizuno, M. Poly(N-phenylglycine)/MoS2 Nanohybrid with Synergistic SolarThermal Conversion for Efficient Water Purification and Thermoelectric Power Generation. *ACS Appl. Mater. Interfaces* **2022**, *14*, 1034–1044.
14. Cui, Y.; Liu, J.; Li, Z.; Ji, M.; Zhao, M.; Shen, M.; Han, X.; Jia, T.; Li, C.; Wang, Y. Donor–Acceptor-Type Organic-Small-Molecule-Based Solar-Energy-Absorbing Material for Highly Efcient Water Evaporation and Thermoelectric Power Generation. *Adv. Funct. Mater.* **2021**, 2106247.
15. Yan, Y.; Zhang, N.N.; Si, J.W.; Li, Z.Y.; Krautscheid, H. Bidirectional $\pi - \pi$ stacking for near-infrared photothermal effects and photo-thermo-electric conversion in a semiconductive hydroxamate coordination polymer. *Chem. Eng. J.* **2024**, *491*, 152054.
16. Yan, Y.; Li, Z.Y.; Zhang, N.N.; Krautscheid, H. A π−π stacked porous framework for highly efficient second near-infrared photothermal effects and photo-thermo-electric conversion. *Chem. Eng. J.* **2024**, *499*, 156059.
17. Weng, X. L.; Liu, J.Y. Strategies for maximizing photothermal conversion efficiency based on organic dyes, *Drug Discov. Today* **2021**, *26*, 2045−2052.
18. Tang, B.; Li, W. L.; Chang, Y.; Yuan, B.; Wu, Y.; Zhang, M. T.; Xu, J. F.; Li, J.; Zhang, X. A Supramolecular Radical Dimer: High-Efficiency NIR-II Photothermal Conversion and Therapy, *Angew. Chem. Int. Ed.* **2019**, *58*, 15526–15531.
19. Li, J.; Kang, M.; Zhang, Z.; Li, X.; Xu, W.; Wang, D.; Gao, X.; Tang, B.Z. Synchronously Manipulating Absorption and Extinction Coefficient of Semiconducting Polymers via Precise Dual-Acceptor Engineering for NIR-II Excited Photothermal Theranostics, *Angew. Chem. Int. Ed.* **2023**, *62*, e202301617.
20. Liao, J.Z.; Zhu, Z.C.; Liu, S.T.; Ke, H. Photothermal Conversion Perylene-Based Metal–Organic Framework with Panchromatic Absorption Bandwidth across the Visible to Near-Infrared, *Inorg. Chem.* **2024**, *63*, 3327–3334.
21. Pan, H.; Li, S.; Kan, J. L.; Gong, L.; Lin, C.; Liu, W.; Qi, D.; Wang, K.; Yan, X.; Jiang, J. A cruciform phthalocyanine pentad-based NIR-II photothermal agent for highly efficient tumor ablation, *Chem. Sci.*, **2019**, *10*, 8246–8252.
22. Wang, S.; Li, S.; Xiong, J.; Lin, Z.; Wei, W.; Xu, Y. Near-infrared photothermal conversion of stable radicals photoinduced from a viologen-based coordination polymer. *Chem. Commun.* **2020**, *56*, 7399–7402.

23. Gao, D.; Zhang, B.; Liu, Y.; Hu, D.; Sheng, Z.; Zhang, X.; Yuan, Z. Molecular Engineering of Near-Infrared Light-Responsive BODIPY-Based Nanoparticles with Enhanced Photothermal and Photoacoustic Efficiencies for Cancer Theranostics. *Theranostics* **2019**, *9*, 5315–5331.
24. Chen, Y.T.; Zhuo, M.-P.; Wen, X.; Chen, W.; Zhang, K.Q.; Li, M.-D. Organic Photothermal Cocrystals: Rational Design, Controlled Synthesis, and Advanced Application. *Adv. Sci.* **2023**, *10*, 2206830.
25. Zhang, M.; Chen, S.; Bao, A.; Chen, Y.; Liang, H.; Ji, S.; Chen, J.; Ye, B.; Yang, Q.; Liu, Y.; Li, J.; Chen, W.; Huang, X.; Ni, S.; Dang, Li.; Li, M.-D.; Anion-Counterion Strategy toward Organic Cocrystal Engineering for Near-Infrared Photothermal Conversion and Solar-Driven Water Evaporation. *Angew. Chem. Int. Ed.* **2024**, e202318628.
26. Chen, K.K.; Qin, C.C.; Ding, M.J.; Guo, S.; Lu, T.-B.; Zhang. Z.-M. Broadband and strong visible-light-absorbing cuprous sensitizers for boosting photosynthesis. *Proc. Natl. Acad. Sci. USA* **2022**, *119*, e2213479119.
27. Lazorski, Megan, S.; Castellano, Felix N. Advances in the light conversion properties of Cu(I)-based photosensitizers. Polyhedron **2014**, *82*, 57–70.
28. Scaltrito, D. V.; Thompson, D. W.; O'Callaghan, J. A.; Meyer. G. J. MLCT excited states of cuprous bis-phenanthroline coordination compounds. *Coord. Chem. Rev.* **2000**, 208243–266.
29. Munakata, M.; Kuroda-Sowa, T.; Maekawa, M.; Honda, A.; Kitagawa, S. Building a Two-dimensional Co-ordination Polymer having a Multilayered Arrangement. A Molecular Assembly comprising Hanging Phenazine Molecules between Polymeric Stair Frameworks of Copper(I) Halides. *J. Chem. Soc., Dalton Trans.* **1994**, 2771–2775.
30. Zhang, N.N.; Liu, Y.T.; Li, L.; Liu, X.T.; Xu, K.; Li, Z.Y.; Yan, Y. Highly efficient NIR-II photothermal conversion from a 2,2′-biquinoline-4,4′-dicarboxylate based photochromic complex, *Inorg. Chem. Front.*, **2024**, *11*, 4867–4875.